Athens Journal of Technology and Engineering - Volume 5, Issue 4 – Pages 337-354

Marine Propeller and Rudder Cavitation Erosion from Full Scale Observations and the Results of a Research Programme

By Ioannis Armakolas[*]
John Carlton[‡]

Ship components such as propellers and rudders are commonly operating in cavitation inducing conditions, therefore they are destined to experience the destructive effects of the phenomenon. Consequently, significant noise, as well as vibrations are commonly reported from ship operators. In addition, propellers and rudders also suffer from cavitation induced erosion, which in some cases can develop even within a few hours of operation, thus the expected service life of those components can be negatively influenced. This paper aims to present an ongoing research programme conducted by the Marine Engineering department of City, University of London which is oriented towards the evaluation of ultrasonically induced cavitation erosion in relation to materials commonly used in propellers and rudders, such as grade DH36 steel, stainless steel 254 and cupronickel 70-30, both from a quantitative and qualitative point of view. As such the relevant experimental procedures that were followed, including mass loss and acoustic emission measurements as well as microscopic and fractographic observations, along with the most important findings, are presented and explained. Results indicate that the proposed experimental procedure can form a baseline upon which efficient and effective evaluation of different materials in relation to ultrasonically induced cavitation erosion can be conducted. Moreover, the development of an acoustic emission – based cavitation erosion monitoring system for rudders, oriented towards the evaluation of erosion both in terms of intensity and location, is also presented. Results, from measurements conducted on small specimens and a reduced-scale model rudder, indicate that the system can potentially be used as means of cavitation erosion monitoring in full scale rudders.

Keywords: *Cavitation erosion, Marine engineering, Non-destructive testing Propeller, Rudder.*

Introduction

Cavitation can be defined as a physical phenomenon characterized by the rapid formation, growth and subsequent collapse of bubbles or cavities, due to large pressure or velocity variations within the affected liquid. The operating conditions of marine propellers and rudders allow for such conditions to develop and as such they suffer from cavitation and its immediate effects. In addition to noise and vibration, cavitation can also result in erosion, thus it is of major importance for ship designers and operators.

The physical phenomenon of cavitation was first mentioned by Euler (1756) who observed a loss of performance in water wheels, whereas the first attempt to

[*]PhD Student, City, University of London, UK.
[‡]Professor, City, University of London, UK.

https://doi.org/10.30958/ajte.5-4-2 doi=10.30958/ajte.5-4-2

describe and analyse the dynamics governing cavitation was made by Besant (1859) in the middle of the 19th century. A little more than a decade later, Reynolds (1873) published a paper where the over-speeding effect of cavitation on propellers was discussed thus he raised awareness regarding the relation of the phenomenon to the marine industry. What he particularly observed was that, the rotational speed of the propeller shaft would rise significantly in the presence of cavitation of considerable intensity. The same over-speeding effect was noted by Sir Charles Parsons in 1894, in his experimental steam turbine propelled vessel called Turbinia (Carlton, 2012). In the beginning of the 20th century, Rayleigh (1917) undertook a significant effort by attempting to analyse the bubble collapse dynamics, thus suggesting a basic cavitation mechanism, followed by Parsons and Cook (1919).

The emergence of high speed photography towards the end of the 20th century, assisted researchers considerably in their effort of understanding the underlying nature of bubble collapsing as well as the resulting erosion of the affected materials. In this context, studies from Philipp and Lauterborn (1998) as well as Lindau and Lauterborn (2003) revealed high pressure waves emitted from collapsing bubbles. Some researchers (Reisman et al., 1998) proposed and demonstrated that depending on the geometry and nature of the cavitation cloud, the resulting shock wave that propagates into the cloud can significantly strengthen towards its centre and as a result the erosive potential of the system increases. In an analogous note, Bark et al. (2004) suggested that for specific geometries the collapse energy of a large cavity can be oriented into a small region of the adjacent solid surface, thus the erosive potential of the system also increases. Others proposed that macro cavities can be converted into collapsing clouds of micro bubbles emitting erosive shock waves (Fortes – Patella et al., 2004). Despite considerable efforts by numerous researchers, however, the ultimate nature of cavitation induced erosion is still debatable whereas phenomena such as bubble collapse and rebound, micro jet formation, clouds of collapsing micro bubbles and cavitation vortices are believed to be the dominant candidates (Franc and Michel, 2004).

Nevertheless, with regards to the effects of cavitation erosion in terms of the resulting mass loss of the affected materials, it has been suggested that it progresses in four distinct stages. These are the incubation, acceleration, steady state and deceleration phases (Karimi and Martin, 1986). It should be noted, however, that the nature of this suggestion is mostly qualitative whereas prediction of the quantitative aspects of erosion would require a relation considering:

- The pressure field distribution on the surface
- The frequency of cavitation structure collapse
- The level of embrittlement of the material
- The transient temperature of collapse
- The relative electro-potential of the erosion site
- The material mechanical properties

In this context, the research programme that is presented in the following chapters is rather oriented towards the evaluation of the material parameter, than the hydrodynamic aspects of cavitation, by making use of the relevant qualitative and quantitative data. These include mass loss and acoustic emission measurements as well as microscopic and fractographic observations, by means of optical and scanning electron microscopes (SEM), respectively. In addition to the aforementioned procedures, the parameter of acoustic emissions, originating from the affected materials, is explored even further, by investigating whether it can be used as means of cavitation erosion monitoring or not in ship rudders.

Experimental Test Rig – Procedure

Experimental Test Rig

The main aim of this study commanded that, the under experimental investigation, specimens would have to be placed in a cavitating liquid medium (water) thus an appropriate test rig was built, essentially consisting of a plastic water tank, a base plate (bridge) for the specimens and a cavitation excitation source by means of an ultrasonic transducer (Figure 1).

Figure 1. *Illustration of the Experimental Test Rig*

.

The under-investigation specimens, shaped in small rectangular plates, were mounted onto the base plate, positioned at the bottom of tank, which was then filled with fresh water. The head of the ultrasonic transducer (sonotrode) was placed just above each specimen's surface at a predetermined distance of 1mm. The base plate, as well as each specimen, had got markings to ensure correct placement, every time a specimen was taken out for measurements.

With regards to the cavitation excitation source, the operating principle of the ultrasonic transducer is based on the reversed piezoelectric effect thus longitudinal

mechanical oscillations at the tip of the sonotrode are generated by electrical stimulation. The frequency of those mechanical oscillations is set at 20 ± 1 kHz whereas the power output of the ultrasonic transducer can be adjusted throughout the range between 50 and 100% of its maximum power output which is 1000W. The titanium made sonotrode is mounted on the horn of the ultrasonic transducer where it functions as a λ/2 oscillator thus it increases the amplitude of those longitudinal mechanical oscillations up to amplitude of 150μm. Mechanical oscillations of that order transmit pressure fluctuations into the water, of sufficient amplitude to induce erosive cavitation, via the front face of the sonotrode (tip).

In the case of prolonged cavitation exposure and due to heat accumulation, water was recirculated through a larger tank, in order to maintain temperature within the desired range (21 ± 1 ºC).

Experimental Methodology

The gap between each specimen and the sonotrode was set at 1mm and the power output of the ultrasonic transducer at 750W, as those settings were found to induce cavitation of sufficient intensity to cause considerable erosion, in terms of measurable mass loss, while preserving the sonotrode tip.

All specimens were exposed to ultrasonically induced cavitation for a period of five (5) hours whereas mass loss measurements were taken every thirty (30) minutes. Three different alloys were examined:

- Grade DH36 steel
- Stainless steel 254
- Cupronickel 70-30

For statistical reasons, a minimum of five (5) specimens were tested for each one of the examined alloys whereas additional care was taken in order to ensure that all specimens were identical with regards to their dimensions as well as their initial surface roughness.

It should be mentioned that the aforementioned methodology mainly applies for the mass loss measurements as well as the microscopic observations, both through an optical and a scanning electron microscope (SEM), which form the main body of this research. Although an analogous methodology was followed in relation to acoustic emission measurements and the cavitation erosion monitoring system any specialized techniques that were applied in these instances will be presented and explained in the relevant chapters.

Mass Loss Measurements

All alloys were exposed to ultrasonically induced cavitation for a period of five (5) hours under identical experimental conditions. Results were plotted onto a graph for comparison reasons, however, it should be noted that the presented data corresponds to the mean values relating to five (5) specimens for each one of the examined alloys (Figure 2).

Figure 2. *Mass Loss Comparison between Grade DH36 Steel, Stainless Steel 254 and Cupronickel 70-30*

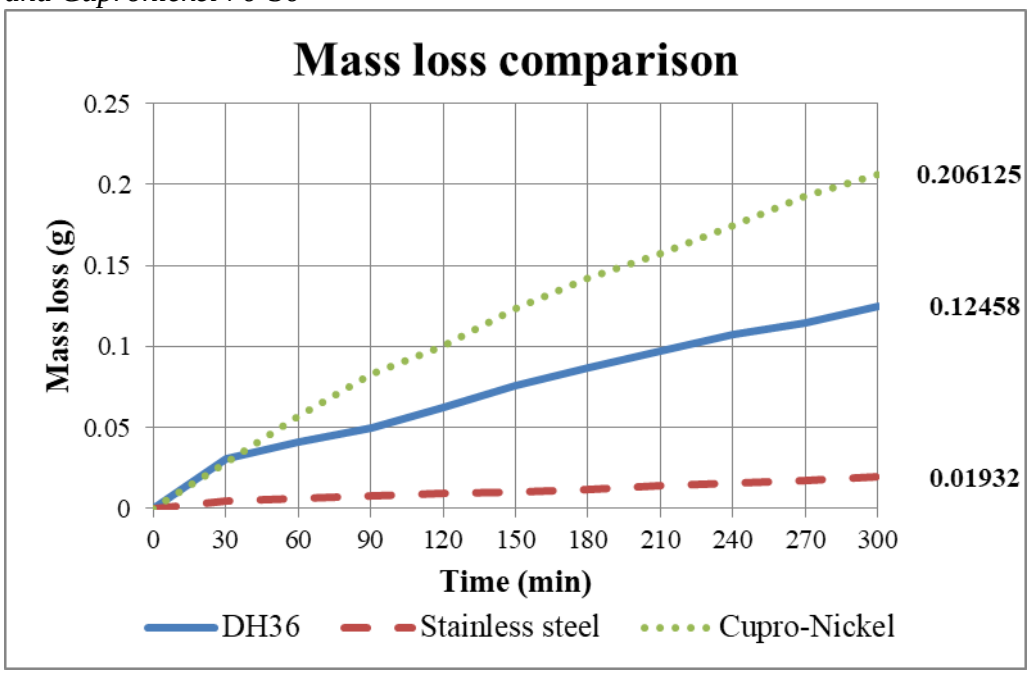

It can be clearly seen that, in general, there is an increase in terms of mass loss for all examined alloys due to continuous ultrasonically induced cavitation exposure. Different slopes with regards to the mass loss lines, however, indicate dissimilar rates of mass loss, between the alloys.

The accumulated mass loss at the end of the five (5) hours exposure due to ultrasonically induced cavitation was:

- 0.01932g for stainless steel 254
- 0.12458g for grade DH36 steel
- 0.206125 for cupronickel 70-30

Results indicate that, with regards to the measured mass loss, stainless steel 254 was remarkably resistant against ultrasonically induced cavitation erosion, followed by grade DH36 steel and cupronickel 70-30.

Interestingly, grade DH36 steel and cupronickel 70-30 exhibited an identical behaviour for the first thirty (30) minutes of exposure, with regards to the measured mass loss. Nevertheless, grade DH36 steel demonstrated a more resistant nature compared to cupronickel 70-30, for the rest of the procedure, possibly due to work hardening effects and different properties.

Microscopic and Fractographic Observations

In addition to quantitative mass loss measurements, specimens were also examined from a qualitative point of view. As such, microscopic and fractographic

observations were conducted, in order for the characteristics of ultrasonically induced cavitation erosion, in relation to each alloy, to be identified and revealed.

Initially, all eroded alloys were examined under the lens of a digital optical microscope under a x500 magnification in order for some general observations regarding the dominant type of fracture (brittle or ductile) to be made (Figure 3).

Figure 3. *Microscopic Appearance of All Eroded Alloys* (Top left) *Grade DH36 Steel* (Top right) *Cupronickel 70-30* (Bottom) *Stainless Steel 254*

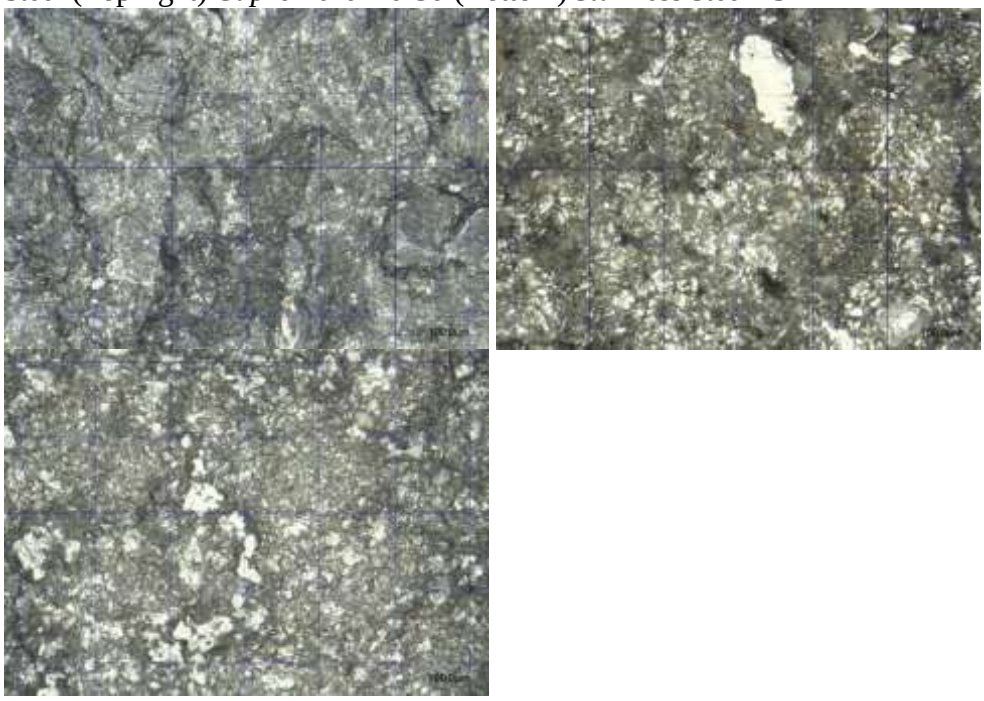

By examining the relevant microscopic images, it was found that the eroded surface of stainless steel 254 was granular whereas it was dominated by characteristics such as sharp bumps and distinctive reflective facets, thus indicating that fracture was mostly brittle in nature. The same apply for grade DH36, where well-defined facets as well as nearly straight edges dominated the erosion pattern, thus indicating an extensive amount of brittle fracture. In this case, however, signs of plastic deformation were also apparent, in the form of small ductile dimples. Finally, the eroded surface of cupronickel 70-30 revealed an almost equal number of signs of both brittle fracture and plastic deformation. In particular, well-defined reflective facets in conjunction with ductile dimples were apparent all over its eroded surface.

Following, the initial microscopic observations, through which an estimation regarding the fracture type (brittle or ductile) was made, eroded specimens were then examined by means of a scanning electron microscope (SEM) in order for, initial estimations to be confirmed as well as the fractography of the eroded surfaces to be explored (Figure 4).

Figure 4. *SEM Images of All Eroded Alloys* (Top) *Grade DH36 Steel* (Middle) *Cupronickel 70-30* (Bottom) *Stainless Steel 254*

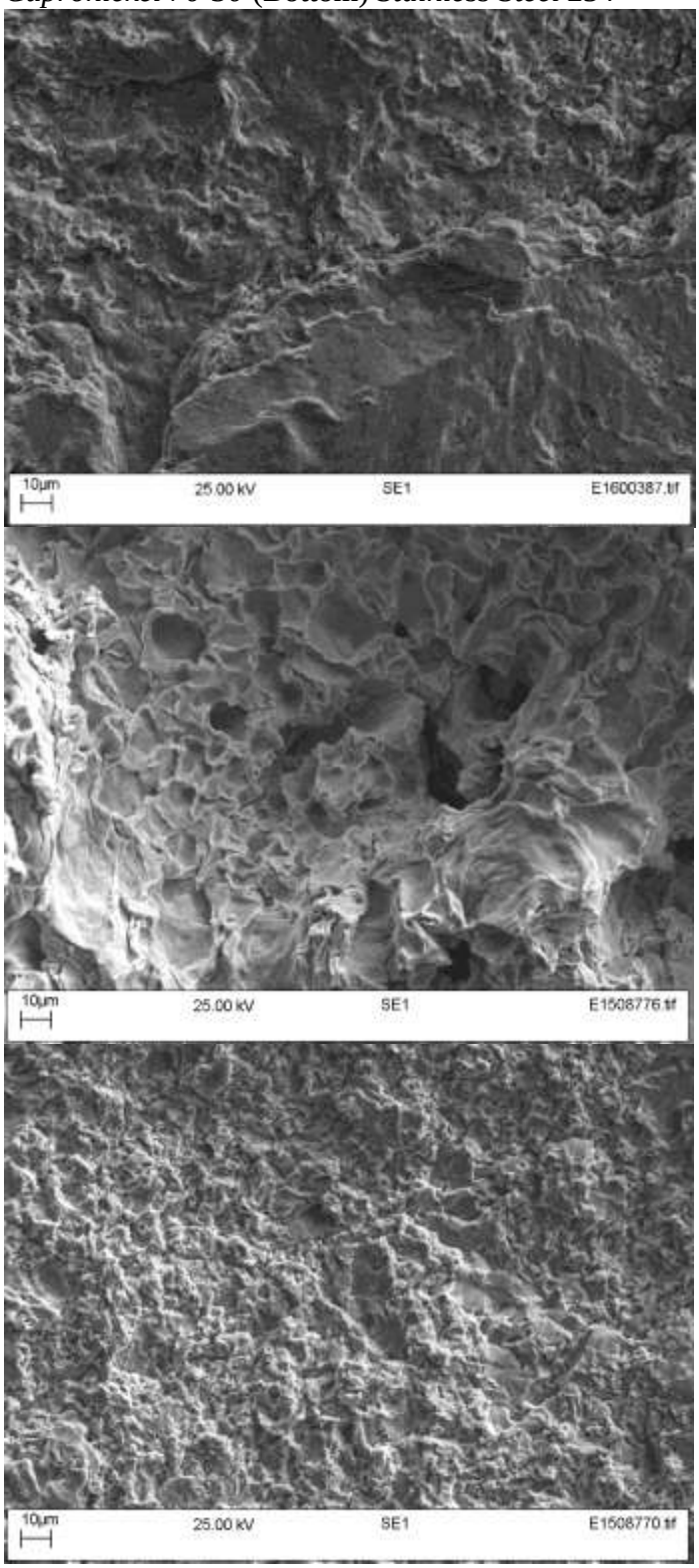

In general, examination of the SEM images confirmed all initial estimations regarding the observed fracture types (brittle or ductile), nevertheless, with the addition of some noteworthy remarks, relating to the fractography of each one of the examined materials.

In the case of cupronickel 70-30 for instance, signs of plastic deformation in the form of ductile dimples of all sizes were clearly apparent all over its surface. Signs of brittle fracture could not be identified as clearly although they were possibly apparent in areas, closely resembling the individual grains of the materials, in the form of intergranular brittle fracture (crack propagation through the grain boundaries). The surface of stainless steel 254 on the other hand was mostly dominated by signs of trangranular (crack propagation through the grains) and to a lesser extent intergranular brittle fracture. The former is characterized by ridges and smooth bumps, whereas the latter is characterized by well-defined facets. Signs of plastic deformation were also apparent, in the form of isolated tiny ductile dimples. On a similar note, signs of mostly transgranular and to a lesser extent intergranular brittle fracture dominated the surface of grade DH36 steel, in the form of ridges and well-defined facets, respectively, however, in comparison to stainles steel, the appereance of those ductile dimples was more frequent thus indicating an increased amount of plastic deformation.

In general, microsopic and SEM observations were in good agreement, while there appears to be a connection between the accumulated mass loss and the observed fracture patterns. In particular, it appears that, increased amounts of mass loss are possibly related to plastic deformation, as it was the case for cupronickel 70-30, whereas the opposite is also true, as it was represented by stainless steel 254, for which characteristics of mostly brittle fracture were observed. Grade DH36 steel, which can be ranked between cupronickel 70-30 and stainless steel 254, with regards to measured mass loss due to ultrasonically induced cavitation erosion, exhibited signs of both brittle fracture and plastic deformation, fact that further reinforces the aforementioned assumption.

Acoustic Emission Measurements

Acoustic emissions can be defined as the elastic stress waves produced by materials when they absorb and release strain energy and stress. In particular, plastic deformation as well as crack growth and propagation are the primary sources of acoustic emissions in metals (Rogers, 2001). Following the first official report of acoustic emissions relating to a metal undergoing stress loading by Portevin and Le Chatelier (1923), acoustic emissions have been studied extensively and are widely used for non-destructive monitoring purposes in structures such as bridges and historical buildings (Carpinteri et al., 2007). In addition, the fact that an acoustic emission based monitoring can be operated remotely and accurately, has contributed significantly to a continuous interest from the relevant industries (Tan et al., 2009).

In this context, it was decided that the parameter of acoustic emissions in relation to the exposure of the examined materials to ultrasonically induced cavitation erosion should also be explored. As such all examined materials, were

exposed to ultrasonically induced cavitation, similarly to the mass loss measurements, although in this case various experimental conditions were examined. In particular, four (4) different test rig configurations were examined, leading to cavitation of varying erosive intensity, in terms of measured mass loss, ranging from non-erosive to highly erosive, whereas in the meantime, the resulting acoustic emissions originating from the exposed materials were monitored.

Acoustic emissions were measured by means of a system based on piezoelectric acoustic sensors whereas the use of fibre Bragg gratings (FBG) was also explored. Piezoelectric sensors operate on the principle of piezoelectricity, which is the ability of some materials to produce an electrical charge in response to mechanical stress (Gautschi, 2002), whereas fibre Bragg gratings are essentially optical sensors that reflect a specific wavelength of light and transmit all others, thus any induced mechanical strain results into a reflected – wavelength shift that can be measured (Othonos and Kalli, 1999). FBGs can especially be utilized in harsh environments due to their immunity to electromagnetic interference, small size, cost and chemical inertness (Mihailov, 2012; Tsuda et al., 2013). They have even been installed in an experimental marine propeller with promising results (Javdani et al., 2016). Piezoelectric acoustic sensors can be used either actively, thus the sensors would generate ultrasonic signals (Giurgiutiu, 2003) or passively, thus the sensors would detect ultrasonic signals (Mal et al., 2003) which is the case in this study.

The acoustic emission monitoring system that was assembled for this study, can be seen in Figure 5, showing both piezoelectric and FBG elements.

Figure 5. *The acoustic Emission Monitoring System*

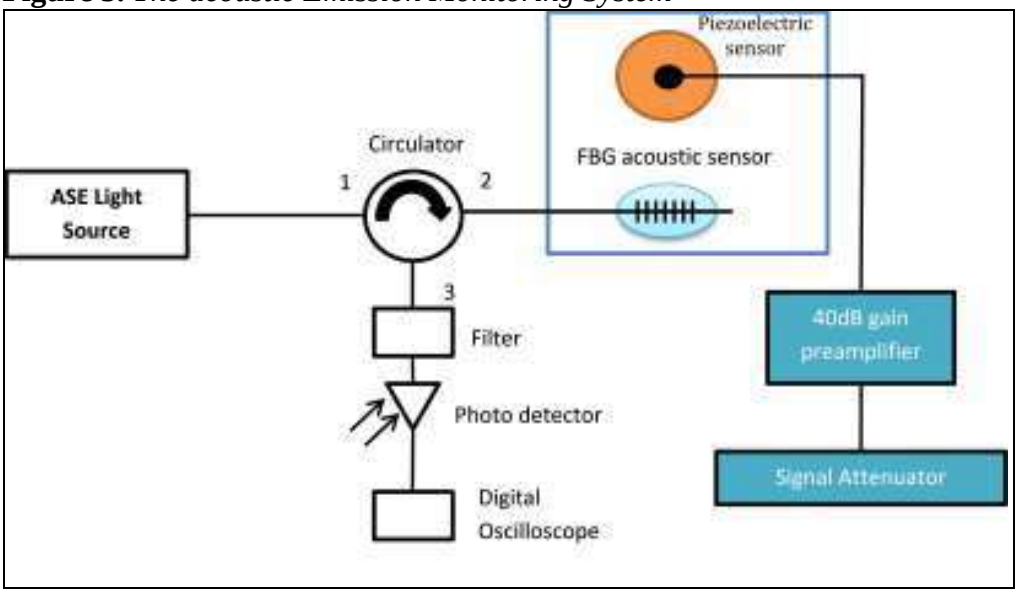

Results for each one of the alloys were plotted onto dedicated graphs, each one containing acoustic data, in terms of acoustic power, for four (4) different test rig configurations (Figure 6). In addition, a fast Fourier transform (FFT), relating to signals from both piezoelectric and FBG sensors is also presented,

in order for the ability of the FBG elements to detect cavitation erosion related signals to be demonstrated (Figure 7).

Figure 6. *Acoustic Emission Measurements*

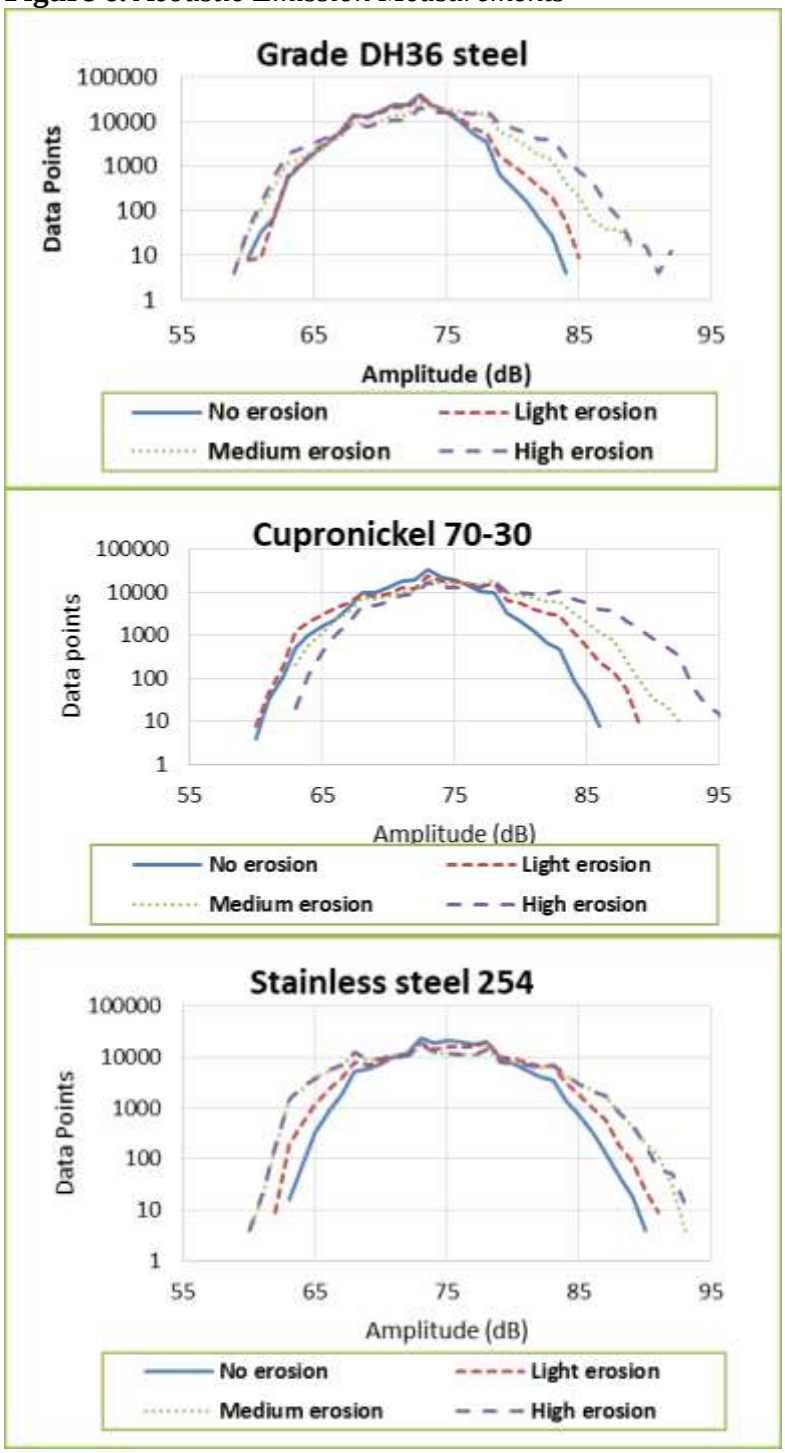

Figure 7. *Frequency Response of Piezoelectric and FBG Elements through the 0-100 kHz Range*

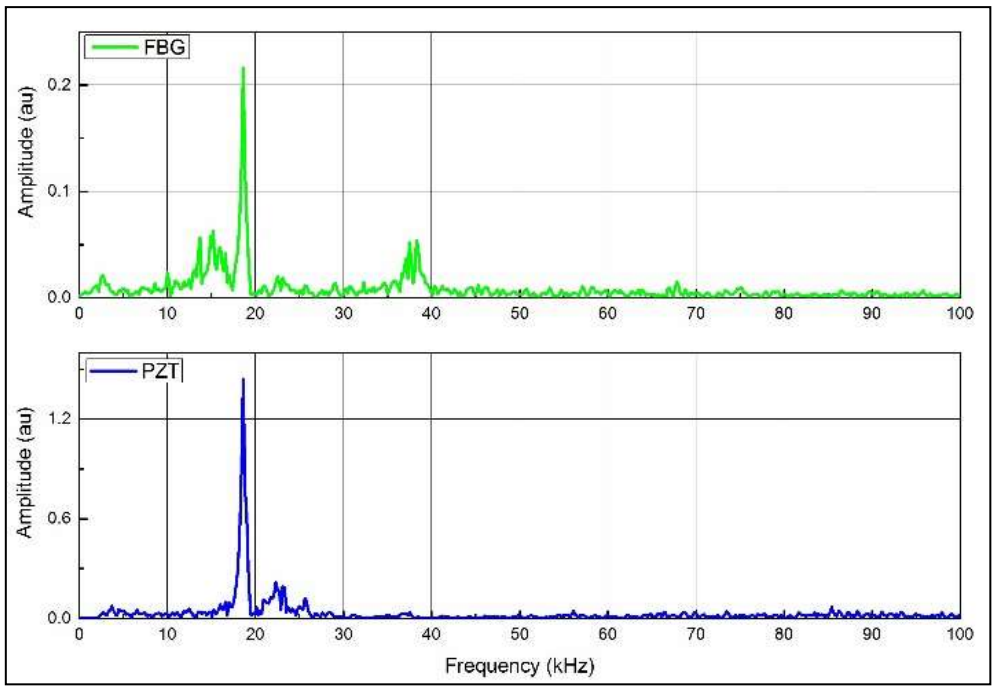

With regards to acoustic emission data, it can be seen that the transition point between 'non-erosive' and 'erosive' cavitation can be clearly identified for all alloys. In particular, the transition point for grade DH36 steel is 85 dB in terms of acoustic power units, whereas for cupronickel 70-30 and stainless steel 254, the relevant values are of the order of 89 and 91 dB, respectively. Acoustic emissions for the 'non-erosive' test rig configurations are of the order of 84 dB for grade DH36 steel, 86 dB for cupronickel 70-30 and 90 dB for stainless steel, thus it appears that the difference between a 'non-erosive' and 'erosive' configuration would be 1 dB for the steel alloys and 3 dB for cupronickel in this instance. The variation between steel alloys and cupronickel as well as the dissimilarities with regards to the absolute values of the resulting acoustic emissions could possibly be attributed to the different properties and internal structure of the examined materials, resulting into a different sort of response against ultrasonically induced cavitation erosion. Nevertheless, one could interpret the results in terms of acoustic erosion 'thresholds' relating to ultrasonically induced cavitation as well as the examined alloys, mainly because the transition point between 'non-erosive' and erosive' cavitation was clearly identifiable, in all instances.

Finally, with regards to the frequency response which is presented in Figure 7 it can be clearly seen that there is a 19.5 kHz resonance which dominates the spectra, in conjunction with a few harmonics, and matches the operating frequency of the ultrasonic transducer. The detected resonance, however, originated from the exposed material itself, thus it is directly related to its internal response against the ultrasonically induced cavitation erosion. It is noteworthy that both types of acoustic sensors, namely piezoelectric and fibre Bragg gratings, were capable of clearly detecting that signal. Although this was in a way expected with regards to

the piezoelectric elements, in the case of fibre Bragg gratings it shows that they can be potentially be used for acoustic emission monitoring purposes.

Cavitation Erosion Monitoring System

Following the successful application of acoustic emissions as means of erosion monitoring for ultrasonically induced cavitation, it was decided that the parameter of erosion localization should also be explored. Towards that direction a reduced-scale model of a ship rudder was designed and built by grade DH36 steel. The reduced-scale rudder model was then exposed to ultrasonically induced cavitation, by following a similar to the other measurements procedure, although in this case other parameters had to be taken into account as well. For instance, the size of the model rudder commanded that a larger tank should be utilized whereas the nature of the acoustic measurements would demand acoustic insulation of the examined object. As such tests were conducted in a large tank whereas the reduced-scale rudder model was positioned into that tank by means of two elastic cables. The test rig configuration as well as the reduced-scale rudder model can be seen in Figure 8.

Figure 8. (Left) *The Reduced-Scale Model Rudder Positioned inside the Large Water Tank* (Right) *The Reduced-Scale Rudder Model*

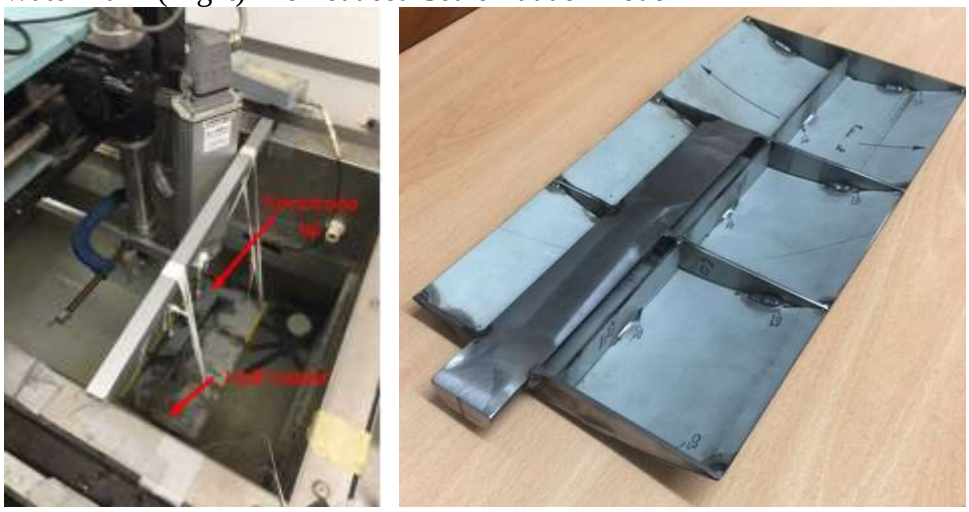

Cavitation erosion localization was conducted by means of a technique based on the principle of triangulation as this was described by Tobias (1976). The basis of this technique lies on an array of three acoustic sensors, located at points S_o (0,0), S_1 (x_1, y_1) and S_2 (x_2, y_2) as well as the acoustic emission source to be located lying at the unknown point P (x,y) at a distance *r* from sensor S_o. An acoustic emission event would then lead to a set of time differences δ_1 and δ_2:

$$\delta_1 = PS_1 - PS_0 = t_1 \, x \, v \quad (1)$$

$$\delta_2 = PS_2 - PS_0 = t_2 \, x \, v \quad (2)$$

where *v* stands for the velocity with which sounds propagates in the material and t_1, t_2 stand for the measured time differences with regards to the arrival of the sound waves for the pairs of sensors S_1-S_0 and S_2-S_0, respectively.

Under those remarks the acoustic emission source P (x,y) would be located at the intersection of three circles with a radius of r, r + δ_1 and r + δ_2 whereas the centre of those circles would be located at points S_o (0,0), S_1 (x_1, y_1) and S_2 (x_2, y_2), respectively. An illustration showing the application of this technique on the surface of the reduced-scale rudder model can be seen in Figure 9.

Figure 9. *The Application of the Triangulation Technique on the Surface of the Reduced Scale Rudder Model*

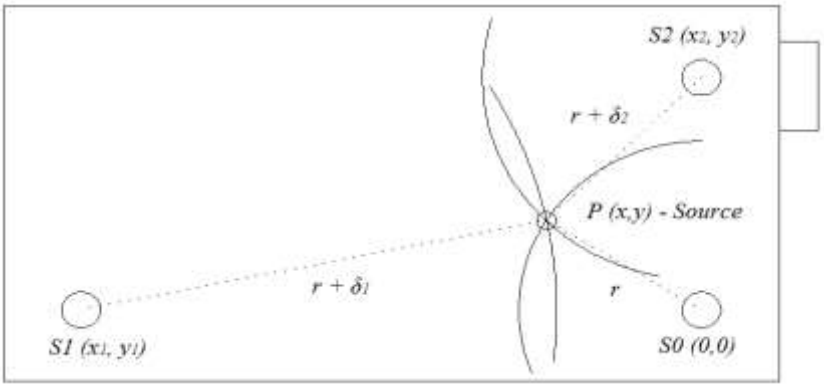

A total of four (4) acoustic sensors, piezoelectric and FBG, were used in these series of tests, as it was stated that the presence of a fourth sensor can greatly increase the accuracy of the triangulation technique. Moreover, eleven (11) different sonotrode placements dispersed all over the upper surface of the reduced-scale rudder were examined. The analytical solution of the sets of equations describing the aforementioned circles leads to the derivation of the coordinates of the intersection point – acoustic source for the eleven (11) different sonotrode placements. Results, for both the piezoelectric and fibre Bragg grating sensors, can be seen in a visualized form through Figure 10.

Figure 10. *Visualization of the Calculated Sonotrode Placements*

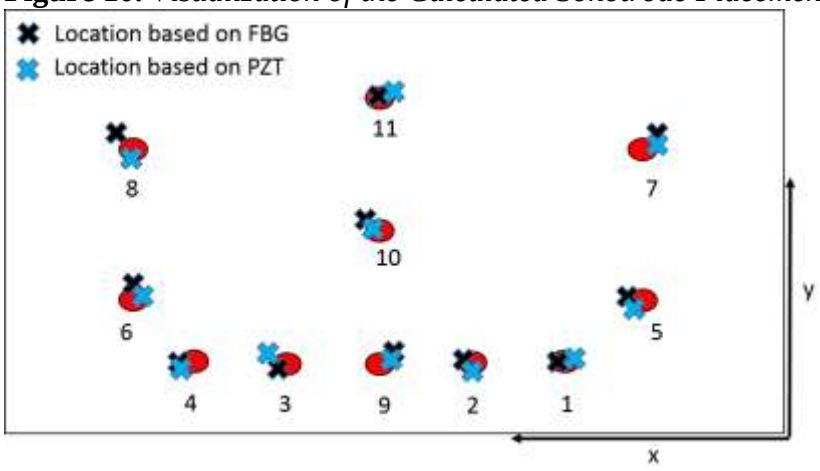

Red dots represent the coordinates of the actual location of the sonotrode.

In all cases, piezoelectric and fibre Bragg grating acoustic sensors proved to be capable of locating the source of erosive cavitation on the surface of the reduced-scale rudder model. Variations between the sensors and the actual coordinates of the sonotrode are possibly related to minor reflections of the resulting acoustic waves due to the presence of the shaft as well as the stringers inside the rudder. Furthermore, the required post-signal filtering could had also slightly influenced the accuracy of the calculations.

Discussion

With regards to the examined materials and in terms of the resulting erosion – mass loss against ultrasonically induced cavitation, stainless steel 254 exhibited the best behaviour followed by grade DH36 steel and cupronickel 70-30. That difference could possibly be explained by the different mechanical properties of the materials, with stainless steel 254 for instance having a tensile strength of the order of 680 MPa whereas the relevant values for grade DH36 steel and cupronickel 70-30 are 490 MPa and 360 MPa, respectively. It is also noteworthy that grade DH36 steel and cupronickel 70-30 lost the same amount of mass after 30 minutes of cavitation exposure, thus exhibited an identical behaviour. Nevertheless, from this point to the end of the procedure grade DH36 steel performed better in the sense that it was constantly losing less mass compared to cupronickel 70-30 whereas its accumulated mass loss after five (5) hours was also significantly lower.

Microscopic examination under the lens of the optical microscope revealed that, the steel alloys suffered from fracture of a more brittle nature, as it was represented by several well-defined facets, whereas cupronickel revealed signs of severe plastic deformation in the form of large ductile dimples. Further examination by means of a scanning electron microscope (SEM) essentially confirmed the aforementioned assumptions whereas it also revealed some additional characteristics relating to the way cracks propagated inside the examined materials. In particular, the presence of numerous bumps and ridges on the surfaces of grade DH36 steel and stainless steel 254 suggested that transgranular (crack propagation through the grains) brittle fracture was the dominant mode whereas the presence of well-defined facets suggested that intergranular (crack propagation through the grain boundaries) fracture also took place although to a lesser extent. Some signs of plastic deformation were also apparent in both cases, in the form of small and isolated ductile dimples. Cupronickel 70-30 in contrast, exhibited a different behaviour, with its surface being characterized by severe plastic deformation in the form of ductile dimples of all sizes whereas an amount of intergranular brittle fracture could also be present in the form of facets closely resembling the grains of the material. Similar to the mass loss measurements, there was good correlation between the mechanical properties of the materials and the resulting erosion, in the sense that strong alloys such as grade DH36 steel and stainless steel 254 exhibited fracture of a more

brittle nature whereas cupronickel 70-30 which can be not be regarded as strong when compared to other two suffered from severe plastic deformation. This is in good agreement with mass loss measurements too, as high amounts of mass loss were accompanied by plastic deformation whereas the opposite behaviour was characterized by fracture of a more brittle nature.

Acoustic emission measurements demonstrated that they can potentially be used as means of monitoring against ultrasonically induced cavitation erosion. The transition point between 'non-erosive' and 'erosive' cavitation was clearly identifiable in all cases, as differences ranging from 1 to 3 dB were measured, in relation to those conditions, for all examined alloys. The absolute values of the resulting acoustic emissions as well as the observed differences between different cavitation conditions appear to be related to the individual properties of each material in addition to cavitation intensity. As for fibre Bragg gratings, they demonstrated that they are at least capable of detecting cavitation, although more research would be required if one would wish to speak in terms of cavitation erosion intensity by means of those sensors.

Finally, localization of ultrasonically induced cavitation erosion on the surface of a reduced-scale model rudder, by means of triangulation, proved to be effective. Both types of acoustic sensors, namely piezoelectric and fibre Bragg gratings, successfully detected the source of cavitation, whereas small discrepancies are believed to be mostly related to the internal structure of the rudder and the required signal filtering.

Conclusions

Cavitation induced by ultrasonic means proved to be an effective experimental method in the sense that results are highly reproducible whereas the resulting intensity is of sufficient amplitude to induce erosion to the adjacent materials. In addition, parameters such as the power output of the ultrasonic transducer or the amplitude of the oscillation as well as the gap between the specimen and the sonotrode are fully adjustable, thus the test rig can be adjusted as desired, leading to cavitation of highly varying intensity. As such, the method that is described in this paper can form a baseline upon which assessment of different materials with respect to ultrasonically induced cavitation erosion can be made. In particular, the behaviour of three alloys against ultrasonically induced cavitation was successfully characterized in terms of the relevant quantitative and qualitative data.

In addition, acoustic emissions were successfully utilized, for cavitation erosion monitoring, initially in the case of small specimens and eventually on a model rudder. In the latter case, apart from the parameter of cavitation erosion intensity, the parameter of cavitation localization was also considered by means of a triangulation technique.

As such, and in conjunction with cavitation erosion intensity measurements, this technique could form the basis of a complete cavitation erosion monitoring system for rudders as well similar components.

Acknowledgements

The authors would like to thank Professor Tong Sun and Mr. Miodrag Vidakovic for their support and assistance throughout this research programme.

References

Bark, G., Berchiche, N. and Grekula, M. 2004. *Application of principles for observation and analysis of eroding cavitation*. EROCAV Observation handbook, Ed. 3.1. Chalmers University of Technology, Sweden.

Besant, W. 1859. *Hydrostatics and Hydrodynamics*. Cambridge University Press.

Carlton, J. 2012. *Marine Propellers and Propulsion*, Ed. 3. Butterworth-Heinemann.

Carpinteri, A., Lacidogna, G. and Pugno, G. 2007. Structural damage diagnosis and life-time assessment by acoustic emission monitoring. *Engineering Fracture Mechanics*, 74, 273-289.

Euler, M. 1756. *Théorie plus complete des machines qui sont mises en movement par la reaction de l'eau* [The most complete theory of machines that are set in motion by the reaction of water]. L'Académie Royale des Sciénces et Bélles Léttres, Berlin.

Fortes-Patella, R., Reboud, J. L. & Briancon-Marjollet, L. 2004. *A phenomenological and numerical model for scaling the flow aggressiveness in cavitation erosion*. Cavitation Erosion Workshop, Val de Rueil, France.

Frank, J. P. & Michel, J. M. 2004. *Fundamentals of cavitation*. Springer Netherlands.

Gautschi, G. 2002. *Piezoelectric sensorics: Force Strain Pressure Acceleration and Acoustic Emission Sensors Materials and Amplifiers*. Springer Berlin Heidelberg.

Giurgiutiu, V. 2003. Lamb wave generation with piezoelectric wafer active sensors for structural health monitoring. *Proceedings of SPIE 5056*, 111-122.

Javdani, S., Fabian, M., Carlton, J., Sun T. and Grattan, K. T. V. 2016. Underwater free-vibration analysis of full-scale marine propeller using a fibre Bragg grating-based sensor system. *IEEE Sensors J.*, vol. 16 (4), 946-953.

Karimi, A. and Martin, J. L. 1986. Cavitation erosion of materials. *International Metals Reviews*, 31, 1-26.

Lindau, O. and Lauterborn, W. 2003. Cinematographic observation of the collapse and rebound of a laser-produced cavitation bubble near a wall. *Journal of Fluid Mechanics*, 419, 327-348.

Mal, A. K., Ricci, F., Gibson, S. and Banerjee, S. 2003. Damage detection in structures from vibration and wave propagation data. *Proceedings of SPIE 5047*, 202-210.

Mihailov, S. J. 2012. Fiber Bragg grating sensors for harsh environments. *Sensors 2012 (12)*, 1898-1918.

Othonos, A. and Kalli, K. 1999. *Fiber Bragg Gratings*. Artech House Inc.

Parsons, C. and Cook, S. 1919. *Trans. Inst. Nav. Arch.*, 61, 233-240.

Philip, A. and Lauterborn, W. 1998. Cavitation erosion by single laser-produced bubbles. *Journal of Fluid Mechanics*, 361, 75-116.

Portevin, A. and Le Chatelier, F. 1923. *Compte. Rendu*, 176, 507-510.

Rayleigh, L. 1917. The pressure developed in a liquid during the collapse of a spherical cavity. *Phil. Mag.*, 34.

Reisman, G. E., Wang, Y-C and Brennen, C. E. 1998. *Observations of Shock Waves in Cloud Cavitation*. J. of Fluid Mechanics, 335, 255-285.

Reynolds, O. 1873. The causes of the racing of the engines of screw steamers investigated theoretically and by experiments. *Trans. INA*.

Rogers, L. M. 2001. *Structural and Engineering Monitoring by Acoustic Emission Methods – Fundamentals and Applications*. Lloyd's Register, Technical Investigation Department.

Tan, A. C. C., Kaphle, M. and Thambiratnam, D. 2009. Structural Health Monitoring of Bridges Using Acoustic Emission Technology. *Proceedings of the 8th International Conference on the Reliability, Maintainability and Safety*, Chengdu, China.

Tobias, A. 1976. Acoustic emission source location in two dimensions by an array of three sensors. *Nondestructive Testing*, 9, 9-12.

Tsuda, H., Sato, E., Nakajima, T. and Sato, A. 2013. Fiber optic sensor technology: An overview. *Sens. Actuators A. Phys*, vol. 82, 40-61.